Iraqi National Journal of Earth Science
www.earth.mosuljournals.com

Land Surface Temperature Estimation from Landsat Thermal Infrared Imagery in Karbala, Iraq

Marwa Razzaq Aya [1*], Athraa Abbas Kadhim[2]

[1] *Department of Reconstruction and Projects, University of Baghdad, Baghdad, Iraq.*
[2] *Technical Institute of Amara, Southern Technical University, Mesan, Iraq.*

Article information

Received: 24- Nov -2023

Revised: 29- Jan -2024

Accepted: 02- May -2024

Available online: 01- Jan – 2025

Keywords:
GIS
Landsat
LST
Remote sensing
Thermal

Correspondence:
Name: Marwa Razzaq Aya
Email:
marwa.r@uobaghdad.edu.iq

ABSTRACT

The land surface temperature (LST) of the Earth is one of the most important factors influencing the exchange of energy and moisture between the Earth's surface and atmosphere. Through this, it can describe the distribution of thermal radiation emitted from the Earth's surface spatially and temporally. LST is critical in many areas and for various purposes, including agriculture, environment, and environmental protection. The primary objective of this study is to study the changes in the temperature of the Earth's surface occurring in Karbala, Iraq, with the help of GIS geospatial techniques to estimate the temperature of the Earth's surface for 2013 and 2023. The Landsat 9 and 8 OLI/TIRS images are processed using the software ArcGIS v10.8. The results show an increase in LST values between 2013 and 2023 of about 4 degrees. The analysis of LST maps show that the minimum temperatures exist in the water bodies, while the maximum temperatures are found in the category of built areas.

DOI: 10.33899/earth.2024.144879.1179,

تقدير درجة حرارة سطح الأرض من مرئيات لاندسات الحرارية بالأشعة تحت الحمراء في كربلاء ، العراق

مروه رزاق عيه [1]*، عذراء عباس كاظم [2]

[1] *قسم الاعمار و المشاريع، جامعة بغداد، بغداد، العراق.*

[2] *المعهد التقني العمارة، الجامعة التقنية الجنوبية، ميسان، العراق.*

معلومات الارشفة

تاريخ الاستلام: 24- نوفمبر -2023

تاريخ المراجعة: 29- يناير -2024

تاريخ القبول: 02- مايو -2024

تاريخ النشر الالكتروني: 01- يناير -2025

الكلمات المفتاحية:

نظم المعلومات الجغرافية

لاندسات

درجة حرارة السطح

الاستشعار عن بعد

الحرارة

المراسلة:

الاسم: مروه رزاق عيه

Email: marwa.r@uobaghdad.edu.iq

الملخص

تعد درجة حرارة سطح الأرض (LST) من اهم العوامل المهمة والمؤثرة على التبادل الحاصل للطاقة والرطوبة بين سطح الأرض والغلاف الجوي. ومن خلاله يمكننا وصف توزيع الإشعاع الحراري المنبعث من سطح الأرض مكانيا وزمانيا. تحمل LST أهمية بالغة في مجالات عدة وفي اغراض متنوعة منها الزراعة والبيئة وحماية البيئة. الهدف الاساسي لهذا البحث هو دراسة التغيرات الحاصلة في درجة حرارة سطح الأرض التي تحدث في كربلاء، العراق، بمساعدة تقنيات GIS الجيومكانية لتقدير درجة حرارة سطح الأرض للعامين 2013 و 2023. اذ اجريت معالجة صورية لمرئيات للقمر لاندسات Landsat 9 و OLI/TIRS 8 باستخدام برنامج ArcGIS v10.8. وبينت هذه النتائج وجود زيادة في قيم LST بين عامي 2013 و 2023 بنحو 4 درجات. واظهر تحليل خرائط LST أن درجات الحرارة الدنيا وجدت في صنف المسطحات المائية، في حين أن درجات الحرارة القصوى وجدت في صنف المناطق المبنية.

DOI: 10.33899/earth.2024.144879.1179,

Introduction

Land surface heat changes are one of the most significant challenges facing the infrastructure of concrete buildings and urban cities. The phenomenon is known as "urban islands", a marked increase in the city's temperature compared to the surrounding villages and rural areas (Blake *et al.*, 2011). This increase can cause several problems, including (Temperature increase, energy consumption, air pollution, and health effects).

Temperature increase: thermal islands absorb and store heat, resulting in higher temperatures within cities in general. This is related to the phenomenon of thermal reflection, as the concretizing surfaces of these buildings, streets, and other solid surfaces reflect heat and produce additional air heating.

Energy consumption: When storing heat, cooling city buildings is important because of high temperatures. This poses an additional burden, resulting in increased electrical power consumption due to the excessive operation of the conditioning devices.

Air pollution: increased temperatures contribute to increased air pollution within urban cities. This is actually due to the cause of warming, then the air situation becomes more stable and then the excess pollution moves more slowly in the atmosphere, after which it accumulates pollutants and in turn affects air quality (Manisalidis *et al.*, 2020).

Health effects: increased temperatures lead to increase heat-related conditions and diseases such as sunstroke, fatigue, thermal fatigue and heat stress (Piracha *et al.,* 2020).

Several solutions and actions can be taken to address these challenges, including planting evergreen trees that bear high temperatures, allocating green spaces within the city's design to reduce heat absorption, cooling and tempering the atmosphere. In addition to enhancing the design of buildings with heat-insulating materials.

Remote sensing and Geographic Information Systems (GIS) are considered pioneering technologies in analyzing the phenomena related to climate changes, such as floods, desertification, and land cover changes (Al-Hussein and Yahyaa, 2019; Sobrino *et al.,* 2014; Wulder *et al.,* 2019). The assessment of land surface temperature (LST) holds a significant importance in various land cover phenomena and environmental studies. Generally, the LST is used to estimate the temperature spatial distribution change, a major climate parameter related to surface energy balance (Stathopoulou and Cartalis, 2007). LST means "the surface temperature that is observed if directly contact or touch it with, also referred to as the skin temperature of the surface". The Land Surface Temperature (LST) is an essential parameter in climate systems, with multiple applications including the examination of the earth's surface energy budget (Le Marshall *et al.,* 2006; Ghada and Sabah, 2021) the prediction of climate patterns (Valor and Caselles, 1996), the analysis of climate variability, the investigation of global sea circulation (Heldens *et al.,* 2023), and the estimation of soil moisture (Rhee *et al.,* 2010). The LST parameter is of great significance in the realm of urban climate research, as emphasized by balance (Li *et al.,* 2013). Numerous studies have been conducted, and diverse methodologies have been suggested to estimate LST using satellite Thermal Infrared (TIR) data through the use of various techniques and algorithms (Olioso, 1995; Qin, 2001). Remote sensing data are suitable for understanding the change in land cover relative to fundamental physical properties in terms of surface radiation and emissivity. Currently, many satellites provide data with global coverage on the thermal band of the spectrum in various spatial and temporal resolutions. For example, the Landsat satellite provided global imagery since 1984. Landsat 8 was launched in 2013 giving continuity to the data record. Landsat 8 satellite acquires thermal data of the Earth's surface by utilizing two specific bands, namely band10 and band11, which possess a spatial resolution of 100 meters. The estimation of surface emissivity from satellite data has been documented by Li et al. (2013). Many methods were proposed to estimate the emissivity based on NDVI. The reason for this phenomenon can be attributed to the strong link observed between the Normalized Difference Vegetation Index (NDVI) and surface emissivity (Jimenez-Munoz et al, 2014; Alsalmany et al, 2023).

The objective of this study is to examine the fluctuations in LST within the region of Karbala, Iraq. Geospatial techniques are employed to analyze the land surface temperature data for the years 2013 and 2023. The utilization of Landsat imagery was observed in the context of Landsat 9 and 8 OLI/TIRS missions, while the processing of satellite imagery is conducted through the application of ArcGIS 10 software.

Study area

Karbala, an Iraqi governorate, has been influenced by Islamic elements, which have significantly contributed to the growth of its urban and population structure. This effect is evident in the organization of land uses inside the city. The city of Karbala is considered one of the archaeological and historical cities in Iraq, as it includes many archaeological sites and holy shrines visited by millions of visitors every year. Over centuries, Karbala has witnessed significant urban change as a result of population growth and economic development. Karbala is located in the Mesopotamian region, specifically positioned to the western side of the Euphrates River in the central part of Iraq. It is positioned around 100 km southwest of Baghdad, with coordinates ranging from 42°- 45°E longitude and 32°-33°N latitude. The total land area of Karbala spans approximately 5,034 km^2 (Al-Madhlom ***et al.,*** 2017). It represents 1.14% of the area of Iraq, which amounts to 438,320 km^2. The study area is geographically next

to the Anbar Governorate to the north and west, the Najaf Governorate to the south, and the Babil Governorate to the east (Fig. 1). Iraq's climate is considered variable and diverse due to its geographical location and the diverse terrain that the country enjoys. Karbala governorate's climate is characterized by a subtropical desert climate, classified under the Köppen climate system under the category BWh. The governorate is subjected to high year-round temperatures, with January being the coldest month with an average minimum temperature of 9.7 °C. The governorate becomes particularly hot in July and August with temperatures reaching 44.7 °C and 44.4 °C respectively (Weather Atlas, 2024), with annual rainfall ranges approximately 11.79 mm (Weather and Climate, 2024).

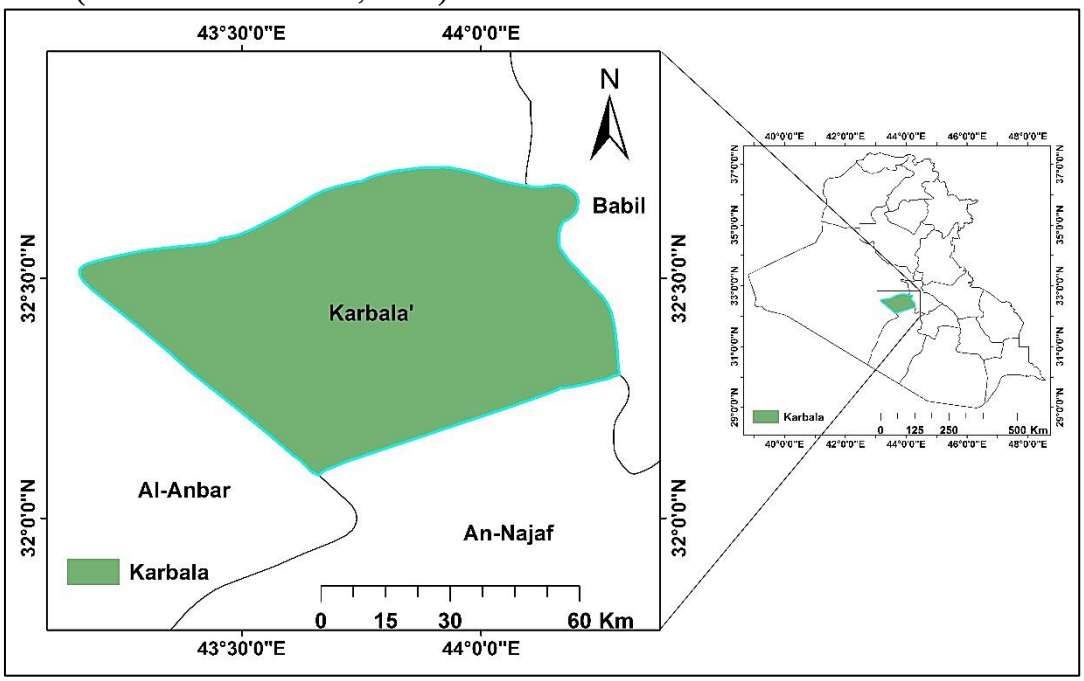

Fig. 1. Location of the study area.

Materials and Methods

Dataset

Since its inaugural flight in 1972, the Landsat satellites have been diligently observing and documenting the Earth's surroundings, thereby establishing a comprehensive and frequently updated worldwide repository of data. Landsat images are extensively utilized as a primary source of remote sensing data due to its notable spatial characteristics, including an optical resolution of 30 meters and thermal resolution ranging from 60 to 120 meters (Table 1). Additionally, Landsat images offer spectral resolution with a minimum of seven bands, incorporating one or two bands dedicated to thermal infrared analysis. Furthermore, Landsat images possess a temporal resolution that allows for returning to the same location every 16 days. Consequently, these distinctive features contribute to the widespread adoption and application of Landsat images in remote sensing studies (Li ***et al.,*** 2023). This study uses Landsat 8 multispectral images to generate LST maps. The image specification is illustrated in Table (2). Cloud-free images are downloaded for September 2013 and 2023.

Table 1: Landsat 8 and 9 bands specifications (NASA, 2024 a, b).

Product	Bands	Wavelength (micrometers)	Spatial resolution (m)
Landsat 8	Band1: coastal/aerosol	0.435 - 0.451	30
	Band 2: Blue	0.452 - 0.512	30
	Band 3: Green	0.533 - 0.590	30
	Band 4: Red	0.636 - 0.673	30
	Band 5: Near Infrared (NIR)	0.851 - 0.879	30
	Band6: SWIR 1	1.566 - 1.651	30
	Band7: SWIR 2	2.107 - 2.294	30
	Band 8: Panchromatic	0.503 - 0.676	15
	Band 9: Cirrus	1.363 - 1.384	30
	Band 10: TIRS 1	10.60 - 11.19	100* 30
	Band 11: TIRS 2	11500-12500	100* 30
Landsat 9	Band1: coastal/aerosol	0.433 - 0.453	30
	Band 2: Blue	0.450 - 0.515	30
	Band 3: Green	0.525 - 0.600	30
	Band 4: Red	0.630 - 0.680	30
	Band 5: Near Infrared (NIR)	0.845 - 0.885	30
	Band6: SWIR 1	1.560 - 1.660	30
	Band7: SWIR 2	2.100 - 2.300	30
	Band 8: Panchromatic	500 - 680	15
	Band 9: Cirrus	1.360 - 1.390	30
	Band 10: TIRS 1	10300 - 11300	100* 30
	Band 11: TIRS 2	11500-12500	100* 30

Table 2: presents the specifications of the Landsat images (https://earthexplorer.usgs.gov/).

Path/Row	Dates	Time	Sun-azimuth	Sun-elevation	Datum
168-37	2013/9	07:28:04	141.373	49.573	WGS84/UTMZone38
168-38	2013/9	07:34:07	139.652	52.165	WGS84/ UTMZone38
169-37	2013/9	07:27:10	142.260	47.630	WGS84/ UTMZone38
169-38	2013/9	07:33:27	144.204	44.372	WGS84/ UTMZone38
168-37	2023/9	07:38:55	138.488	54.694	WGS84/UTMZone38
168-38	2023/9	07:39:19	136.684	55.588	WGS84/ UTMZone38
169-37	2023/9	07:39:04	137.003	56.663	WGS84/ UTMZone38
169-38	2023/9	07:39:27	135.036	57.526	WGS84/ UTMZone38

Estimated LST Using Landsat Data

To estimate the LST using Landsat 8 data for the year 2013, and Landsat 9 for the year 2023, the ArcGIS software is applied following the steps illustrated in Figure (2) below:

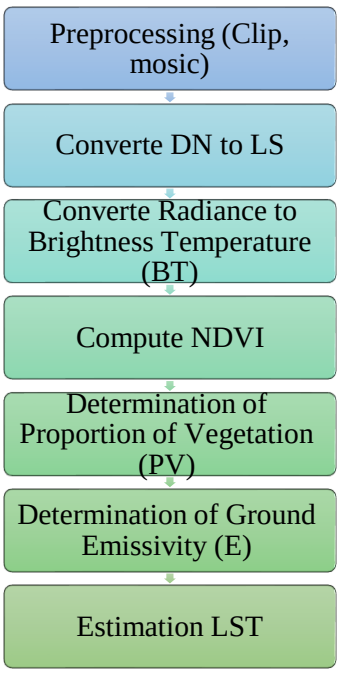

Fig. 2. Methodology to estimate LST using Landsat data.

***Step 1*: Sensor spectral radiance (LS) determination**

The process of converting digital number (DN) data to absolute radiance involves the conversion of pixel values representing the thermal band (B10) into sensor spectral radiance (LS). This step is done using Equation (1) (Walawender ***et al.,*** 2012; Kumar and Shekhar, 2015).

$$LS = gain * DN + bias \quad \text{---------- (1)}$$

where gain = 0.00033420, and bias = 0.100.

***Step 2*: Radiance conversion to at-satellite Brightens Temperature (BT)**

The second step is converting Ls to BT using Equation (2). In this case, the thermal constants of TIR band 10 (K1 = 774.8853, and K2=1321.0789) are utilized, and these constants can be found in the metadata file linked to the satellite images (Walawender ***et al.,*** 2012; Kumar and Shekhar, 2015).

$$BT = \frac{K2}{ln\left(\frac{k1}{L_s}+1\right)} - 273.15 \quad \text{---------- (2)}$$

The thermal constants K1 and K2, which are relevant to thermal infrared radiation (TIR), can be located within the metadata file linked to the satellite images. For the purpose of obtaining temperature measurements in percentage degrees, the concept of absolute zero, which is exactly (-273.15) degrees Celsius, must be integrated.

***Step 3*: Normalized Difference Vegetation Index retrieval:**

The NDVI is a direct quantitative measure used to identify and assess areas of green vegetation that are growing increasingly. This digital index varies in value between (-1 and + 1). In general, the values ranging from 0.8 to 1 indicate the high densities of vegetation, while the values close to 0 indicate the absence of vegetation cover. Table (3) shows the typical NDVI values for different land cover types. The NDVI is calculated at the individual pixel level within the images by measuring the natural variation between the red ranges, which ranges from 0.636-0.673μm to the near-infrared range with values ranging from 0.851-0.879μm. This index calculation of Landsat 8 images includes the use of band 4 representing RED and band 5 representing NIR by applying the equation as follows (Braun and Herold, 2004):

$$NDVI = \frac{NIR-Red}{NIR+Red} \quad \text{---------- (3)}$$

The NDVI index is a scale widely used and common in remote sensing studies and time monitoring of vegetation changes. Where NIR refers to the near-infrared region. The red band is represented by the color red. The calculation of the NDVI for Landsat 8 or 9 imagery involves the utilization of band 4 known as RED and band 5 known as NIR.

Table 3: Typical NDVI values for various cover types (Holben, 1986).

Land cover	NIR	RED	NDVI
Bare soil	0.28	0.27	0.03
Water	0.01	0.02	-0.26
Clouds	0.23	0.23	0.002
Snow	0.34	0.38	-0.05
Dense vegetation	0.5	0.1	0.7

***Step 4:* calculate proportional vegetation (Pv) from NDVI values:**

This methodology provides estimates of the proportion of vegetation within each land cover category. The proportions of vegetation and bare soil are obtained by analyzing the NDVI of pixels that contain only pure vegetation or bare soil. The derivation of vegetation and bare soil proportions is based on the NDVI values obtained from unpolluted pixels. The calculation of Pv can be determined by employing the equation (4) proposed by Zhou et al. (2003):

$$Pv = \left(\frac{NDVI - NDVI\,min}{NDVI\,max - NDVI\,min}\right)^2 \text{ ---------- (4)}$$

The NDVI max is the NDVI for vegetation, while the NDVI mine is the NDVI for soil (Stathopoulou and Cartalis, 2007).

Step 5: **Find the emissivity of the land surface cover:**

The next stage is to find the emissivity of the land surface cover using NDVI measurements. Water bodies exhibit a notably stable emissivity compared to land surfaces. The dependence of emissivity on wavelength allows for the utilization of the NDVI as a means to measure the emissivity of diverse land surfaces within the 10-12 μm wavelength range. The equation below is proposed initially by Ahmed (2013):

$$e = 0.004 \times Pv + 0.986 \text{ ---------- (5)}$$

The variable "e" represents the land surface emissivity derived from NDVI.

Step 6: **Compute LST**

The retrieval of LST can be accomplished by utilizing Equation (6), which relies on the Brightness Temperature (BT) value of the thermal band, the Land Surface Emissivity (LSE) generated from the Vegetation Fraction (Pv), and NDVI (Jiménez-Muñoz, 2014).

$$LST = \frac{BT}{1 + \left(\frac{\lambda BT}{\rho}\right) lnE} \text{ ---------- (6)}$$

The variable denoted as LST represents the land surface temperature measured in degrees Celsius. Meanwhile, λ refers to the average wavelength.

Results and Discussion

This study shows the LST spatial distribution map regarding land cover via NDVI. The NDVI for the study area is shown in Figure (3). Landsat 8 OLI for September 2013 and 2023 is used. All the processing steps are implemented using ArcGIS software. The examination of the Landsat thermal images revealed alterations in LST over the region of Karbala. The temperature range observed in September 2013 varied from 20.5ºC to 45.7ºC. Conversely, in September 2023, the temperature range was recorded as 21ºC to 49.3ºC, as depicted in Figure (4). During the research period, there is a notable rise in LST. Water bodies such as rivers and lakes exhibit the lowest LST, whereas structures demonstrate the largest concentration of LST. There exists a clear correlation between LST and the presence of buildings. Specifically, an increase in the number or size of buildings is associated with higher LST values. Table (4) illustrates the LST statistical data.

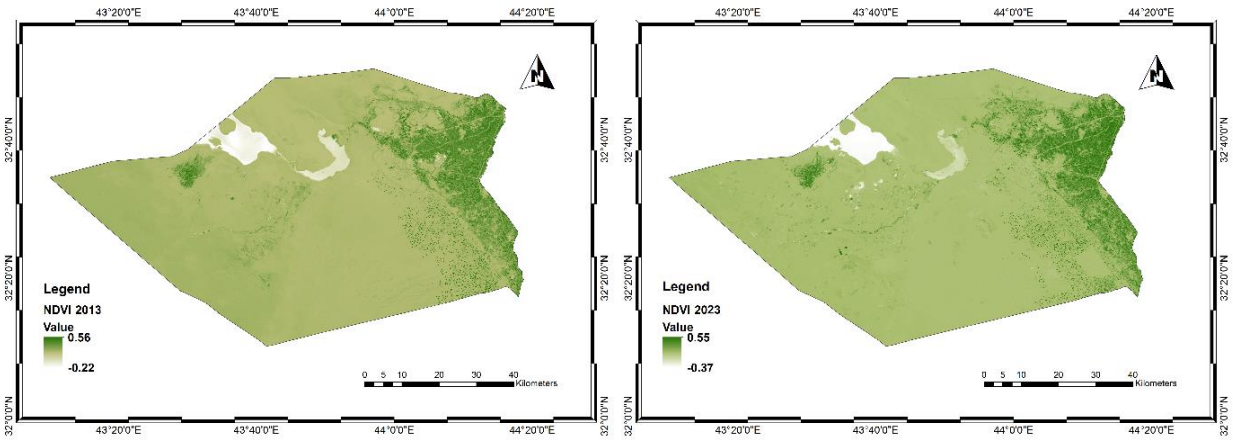

Fig. 3. NDVI for the years 2013 and 2023.

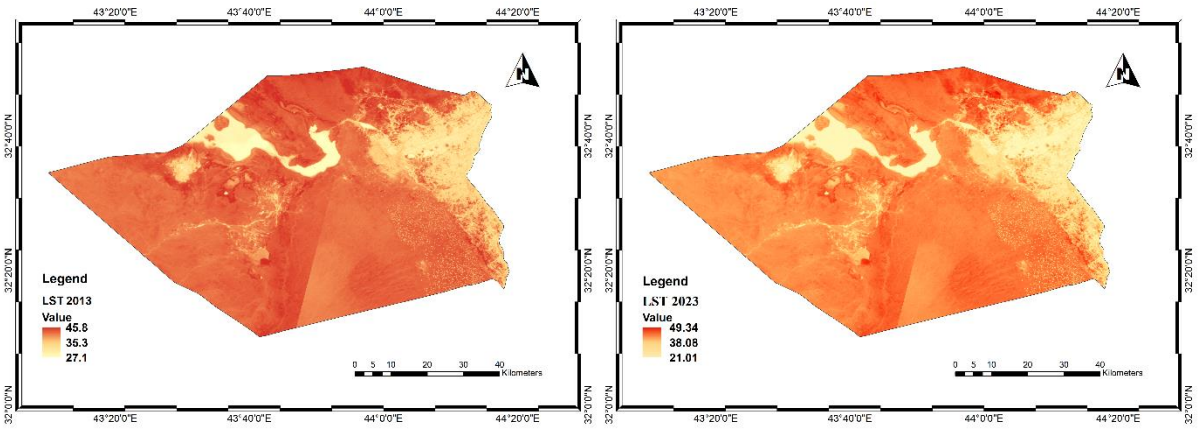

Fig. 4. LST result for the years 2013 and 2023.

Table 4: LST statistical data.

Year	Min. (℃)	Max. (℃)	Mean (℃)	St Deviation (SD)
2013	20.5	45.7	38.1	3.2
2023	21	49.4	39.5	4.3

We notice from figures (3 and 4) that the water bodies are of lowest temperature (about 27 ^{o}C) followed by green areas with a temperature (about 35 ^{o}C) and finally, bare soil and built-up areas are of highest temperature (about 45 ^{o}C). In the year 2023, temperature values increased, and this increase is likely due to increased desertification and water shortages, which negatively affected vegetation cover, as well as increaseing urban expansion in recent years. Analysis shows that all records of the Min., Max., and Mean statistically significant increase about 0.5, 3.7, and 1.4 ^{o}C per decade, respectively. One of the prominent features that emerged from Figure (4) is that the areas located in the urban and suburban areas (at the eastern side of the area) exhibit higher increasing trends in LST values compared with those situated in the rural areas. These clear differences in temperatures are most likely due to land use changes during the study period, especially urban expansion.

Conclusion

The present investigation employes Landsat imagery to assess the alterations in the Land Surface Temperature (LST) for the period spanning from 2013 to 2023. The LST parameter holds significant importance in urban development. Modelling for estimating the LST from Landsat thermal imagery can be considered a good, time-saving, and effective option. The findings suggest a positive correlation between the expansion of urban development and elevated LST, while a negative association is observed between LST and the presence of vegetation. There is an increase in the LST values between 2013 and 2023 of about 4 degrees. An analysis of LST maps reveals that minimum temperatures are found in water bodies which range from (21-27 ^{o}C), while maximum temperatures are in built-up areas which range from (45- 49 ^{o}C).

References

Ahmed, K. A., 2013. Determination of Irrigated Field Units in North Al-Jazeera Irrigation Project Using Remote Sensing Data. Tikrit Journal of Engineering Sciences, 21(2), 68–74. https://doi.org/10.25130/tjes.21.2.09

Al-Hussein, A. and Yahyaa, A., 2019. Morphometric Characteristics of Wadi Koysenjaq Basin in Erbil Using GIS. Iraqi National Journal of Earth Sciences, 19(2), 15–40. https://doi.org/10.33899/earth.2019.170275

Al-Madhlom, Q., Al-Ansari, N., Hussain, H. M., Lindblom, J., Abdullah, T., Abid Hamza, B., and Knutsson, S., 2017. Seepage velocity of Dibdibba formation in Karbala, Iraq. Engineering, 9(3), 279-290. https://doi.org/10.4236/eng.2017.93015

Alsalmany, M. M., Thannoun, R. G. and Shehab, A. T., 2023. Determining the impact of climatic elements on vegetation cover based on remote sensing data- (Al-Hamdaniya district as a case study). *Iraqi National Journal of Earth Science*, *23*(1), 13–25. https://doi.org/10.33899/earth.2022.134400.1017

Blake, R., Grimm, A., Ichinose, T. Horton, R., Gaffin, S., Jiong, S., Bader, D., Cecil, L. D., 2011. Urban climate: Processes, trends, and projections. In Climate Change and Cities: First Assessment Report of the Urban Climate Change Research Network. (Rosenzweig, C., Solecki, W. D., Hammer, S. A., Mehrotra, S., Eds.), Cambridge University Press, Cambridge, UK, 43–81. https:// Doi: 10.1017/CBO9780511783142.009

Braun, M. H. and Herold, M., 2003. Mapping imperviousness using NDVI and linear spectral unmixing of ASTER data in the Cologne-Bonn region (Germany) [Conference presentation]. Remote Sensing for Environmental Monitoring, GIS Applications, and Geology III. Barcelona, Spain. https://doi.org/10.1117/12.510978

Heldens, W., Taubenböck, H., Esch, T., Heiden, U. and Wurm, M., 2013. Analysis of surface thermal patterns in relation to urban structure types: A case study for the city of Munich. Remote Sensing and Digital Image Processing, 17, 475–493. https://doi.org/10.1007/978-94-007-6639-6_23

Holben, B. N., 1986. Characteristics of maximum-value composite images from temporal AVHRR data. International journal of remote sensing, 7(11), 1417-1434. https://doi.org/10.1080/01431168608948945

Jimenez-Munoz, J. C., Sobrino, J. A., Skokovic, D., Mattar, C. and Cristobal, J., 2014. Land surface temperature retrieval methods from landsat-8 thermal infrared sensor data. IEEE Geoscience and Remote Sensing Letters, 11(10), 1840–1843. https://doi.org/10.1109/LGRS.2014.2312032

Jiménez-Muñoz, J. C., Sobrino, J. A., Skoković, D., Mattar, C. and Cristobal, J., 2014. Land surface temperature retrieval methods from Landsat-8 thermal infrared sensor data. IEEE Geoscience and remote sensing letters, 11(10), 1840-1843. https://doi.org/10.1109/LGRS.2014.2312032

Kumar, D. and Shekhar, S., 2015. Statistical analysis of land surface temperature–vegetation indexes relationship through thermal remote sensing. Ecotoxicology and environmental safety, 121, 39-44. https://doi.org/10.1016/j.ecoenv.2015.07.004

Le Marshall, J., Jung, J., Derber, J., Chahine, M., Tredon, R., Lord, S. J., Goldberg, M., Wolf, W., Liu, H. C., Joiner, J., Woollen, J., Todling, R., van Delst, P. and Tahara, Y., 2006. Improving global analysis and forecasting with AIRS. Bulletin of the American Meteorological Society, 87(7), 891–894.https://doi.org/10.1175/BAMS-87-7-891

Li, Z. L., Tang, B. H., Wu, H., Ren, H., Yan, G., Wan, Z., Trigo, I. F. and Sobrino, J. A., 2013. Satellite-derived land surface temperature: Current status and perspectives. Remote Sensing of Environment, 131, 14–37. https://doi.org/10.1016/j.rse.2012.12.008

Li, Z. L., Wu, H., Duan, S. B., Zhao, W., Ren, H., Liu, X., Leng, P., Tang, R., Ye, X., Zhu, J., Sun, Y., Si, M., Liu, M., Li, J., Zhang, X., Shang, G., Tang, B. H., Yan, G. and Zhou, C., 2023. Satellite Remote Sensing of Global Land Surface Temperature: Definition, Methods, Products, and Applications. Reviews of Geophysics, 61(1). https://doi.org/10.1029/2022RG000777

Manisalidis, I., Stavropoulou, E., Stavropoulos, A. and Bezirtzoglou, E., 2020. Environmental and health impacts of air pollution: a review. Frontiers in public health, 8(14), 1-13. https://doi.org/10.3389/fpubh.2020.00014

NASA, 2024a. LANDSAT 8 SPECTRAL SPECIFICATIONS. https://landsat.gsfc.nasa.gov/satellites/landsat-8/

NASA, 2024b. LANDSAT 9 SPECTRAL SPECIFICATIONS. https://landsat.gsfc.nasa.gov/satellites/landsat-9/landsat-9-instruments/landsat-9-spectral-specifications/

Olioso, A., 1995. Simulating the relationship between thermal emissivity and the normalized difference vegetation index. International Journal of Remote Sensing, 16(16), 3211–3216. https://doi.org/10.1080/01431169508954625

Piracha, A. and Chaudhary, M. T., 2022. Urban air pollution, urban heat island and human health: a review of the literature. Sustainability, 14(15), 9234. https://doi.org/10.3390/su14159234

Qin, Z., Karnieli, A. and Berliner, P., 2001. A mono-window algorithm for retrieving land surface temperature from Landsat TM data and its application to the Israel-Egypt border region. International Journal of Remote Sensing, 22(18), 3719–3746. https://doi.org/10.1080/01431160010006971

Rasheed, A. S., Finjan, R. H., Hashim, A. A. and Al-Saeedi, M. M., 2021. 3D face creation via 2D images within blender virtual environment. Indonesian Journal of Electrical Engineering and Computer Science, 21(1), 457–464. https://doi.org/10.11591/ijeecs.v21.i1.pp457-464

Rasheed, A. S., Zabihzadeh, D. and Al-Obaidi, S. A. R., 2020. Large-Scale Multi-modal Distance Metric Learning with Application to Content-Based Information Retrieval and Image Classification. International Journal of Pattern Recognition and Artificial Intelligence, 34(13). https://doi.org/10.1142/S0218001420500342

Rhee, J., Im, J. and Carbone, G. J., 2010. Monitoring agricultural drought for arid and humid regions using multi-sensor remote sensing data. Remote Sensing of Environment, 114(12), 2875–2887. https://doi.org/10.1016/j.rse.2010.07.005

Sobrino, J. A., Jiménez-Muñoz, J. C. and Paolini, L., 2004. Land surface temperature retrieval from LANDSAT TM 5. Remote Sensing of Environment, 90(4), 434–440. https://doi.org/10.1016/j.rse.2004.02.003

Stathopoulou, M. and Cartalis, C., 2007. Daytime urban heat islands from Landsat ETM+ and Corine land cover data: An application to major cities in Greece. Solar Energy, 81(3), 358–368. https://doi.org/10.1016/j.solener.2006.06.014

Valor, E. and Caselles, V., 1996. Mapping land surface emissivity from NDVI: Application to European, African, and South American areas. Remote Sensing of Environment, 57(3), 167–184. https://doi.org/10.1016/0034-4257(96)00039-9

Walawender, J. P., Hajto, M. J. and Iwaniuk, P., 2012, July. A new ArcGIS toolset for automated mapping of land surface temperature with the use of LANDSAT satellite data. In 2012 IEEE international geoscience and remote sensing symposium (pp. 4371-4374). IEEE. https://doi.org/10.1109/IGARSS.2012.6350405

Weather and Climate ,2024. Karbala, Iraq Climate. https://weatherandclimate.com/iraq/karbala

Weather Atlas, 2024. Climate and monthly weather forecast Karbala, Iraq**.** https://www.weather-atlas.com/en/iraq/karbala-climate

Wulder, M. A., Loveland, T. R., Roy, D. P., Crawford, C. J., Masek, J. G., Woodcock, C. E., Allen, R. G., Anderson, M. C., Belward, A. S., Cohen, W. B., Dwyer, J., Erb, A., Gao, F., Griffiths, P., Helder, D., Hermosilla, T., Hipple, J. D., Hostert, P., Hughes, M. J., … Zhu, Z., 2019. Current status of Landsat program, science, and applications. Remote Sensing of Environment, 225, 127–147. https://doi.org/10.1016/j.rse.2019.02.015

Younis, G. G. and Ali, S. H., 2021. Selection of the Optimum Sites for the Wind Turbines Installation in Nineveh Governorate by using GIS. Iraqi National Journal of Earth Science, 21(1), 1–16. https://doi.org/10.33899/earth.2021.170376

Zhou, L., Dickinson, R. E., Tian, Y., Jin, M., Ogawa, K., Yu, H. and Schmugge, T., 2003. A sensitivity study of climate and energy balance simulations with use of satellite-derived emissivity data over Northern Africa and the Arabian Peninsula. Journal of Geophysical Research: Atmospheres, 108(24). https://doi.org/10.1029/2003jd004083